Research Article

Journal of Environmental Nanotechnology

Green Engineering and Sustainable Development of Nitrogen-doped Carbon Quantum Dots (MPE-NCQDs): A Correlative Study of Structure, Composition and Photophysical Properties

Thutipati Appa Rao[1,2], Yeduru Venkatesh[1], Bonige Kishore Babu[2*], Adari Venkata Ramesh[1], N. Sankara Rao[1], R. Ramesh Naidu[3]

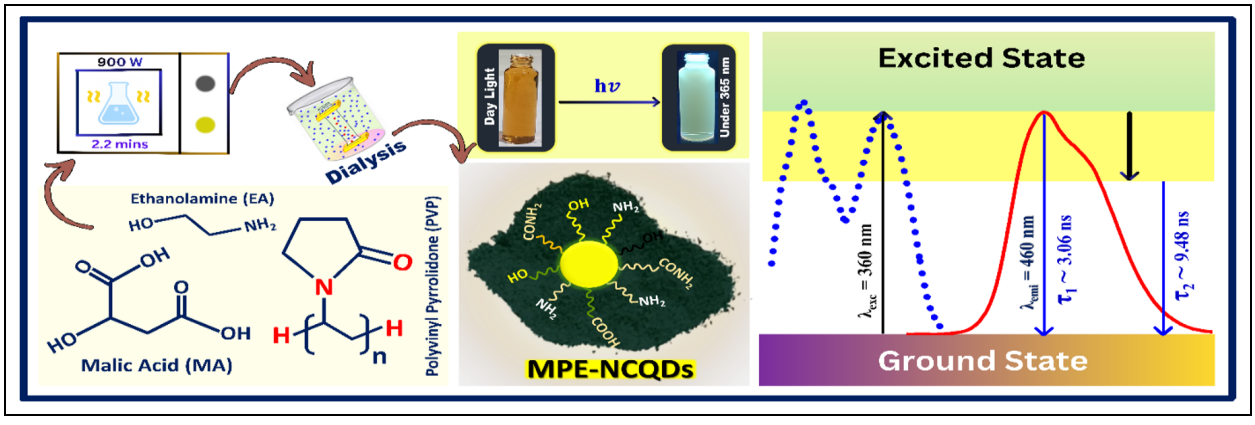
[1]Department of Chemistry, Dr. V. S. Krishna Government Degree College (A), Visakhapatnam, AP, India
[2]Department of Engineering Chemistry, AU College of Engineering, Andhra University, Visakhapatnam, AP, India
[3]Department of Chemistry, Government Degree College, Rajam, Srikakulam, AP, India
Received: 02.01.2026 Accepted: 16.03.2026 Published: 30.03.2026
*dr.bkbabu@andhrauniversity.edu.in

ABSTRACT

A sustainable one-step microwave-assisted strategy is reported for the synthesis of nitrogen-doped carbon quantum dots (MPE-NCQDs) using malic acid as a bio-derived carbon precursor in the presence of polyvinylpyrrolidone and ethanolamine. The approach integrates rapid carbonization with in situ surface passivation and heteroatom incorporation, enabling controlled formation of emissive carbon nanostructures under mild processing conditions. The resulting MPE-NCQDs exhibit uniform nanoscale characteristics, good aqueous dispersibility, and stable photoluminescence, arising from the combined influence of carbon core structure and surface functional chemistry. Systematic structural and photophysical analyses reveal that emission behaviour is governed by the interplay between precursor chemistry, nitrogen configuration, and surface passivation, rather than by size effects alone. By correlating sustainable precursor design with microwave processing and structure–property relationships, this work addresses a key gap in the development of environmentally benign CQD systems. The findings highlight the potential of malic-acid-based, microwave-derived N-CQDs as versatile platforms for optoelectronic and sensing-related applications.

Keywords: Carbon quantum dots; Microwave synthesis; Nitrogen doping; Sustainable precursors; Structure–property correlation.

GRAPHICAL ABSTRACT



1. INTRODUCTION

Carbon quantum dots (CQDs) represent an emerging subclass of zero-dimensional carbon nanostructures whose appeal arises from the convergence of nanoscale confinement, favourable photoluminescence behaviour, and intrinsic biocompatibility. The sub-10 nm dimensions of CQDs impose spatial confinement on charge carriers, leading to excitation-wavelength-dependent emission while simultaneously promoting aqueous dispersibility and chemical stability. (Qiao *et al.* 2020; Elkun *et al.* 2024). Unlike traditional semiconductor quantum dots, CQDs exhibit negligible toxicity, allowing their deployment in

biologically and environmentally relevant applications such as sensing, imaging, and catalytic systems (Wu *et al.* 2017; Derfus *et al.* 2004; Qiao *et al.* 2020). As a result of these combined attributes, CQDs have been actively explored across optoelectronic devices, fluorescence-based sensing platforms, bioimaging systems, photocatalytic processes, and environmental monitoring technologies. (Lin *et al.* 2016; Yuan *et al.* 2020; Pandey *et al.* 2021; Venkatesh *et al.* 2025). The functional performance of CQDs is governed not solely by the dimensions of sp^2-hybridized carbon domains, but by the coupled influence of quantum confinement and surface-state engineering arising from functional groups and heteroatom incorporation to tailor their optical and electronic behaviour. Despite the availability of both bottom-up (hydrothermal, solvothermal, microwave) and top-down (electrochemical, combustion, exfoliation) synthetic strategies, persistent challenges remain in simultaneously achieving high quantum yield, uniform size distribution, reproducible surface passivation, and scalable processing. (Li *et al.* 2010; Lu *et al.* 2011; Stefanakis *et al.* 2014; Sarkar *et al.* 2016; Sasikumar *et al.* 2024; Venkatesh *et al.* 2025). Nevertheless, many existing synthetic strategies suffer from high production costs, complex processing steps, and limited environmental sustainability, underscoring the importance of developing simple, economical, and eco-friendly fabrication routes (Atchudan et al., 2020; Qi et al., 2023).

Among the various chemical modification strategies explored, heteroatom incorporation has proven particularly effective in perturbing the electronic structure of CQDs and modulating their radiative recombination pathways. In particular, nitrogen incorporation is known to introduce additional electronic states, enhance electron-donor characteristics, and improve surface passivation, thereby promoting radiative recombination and increasing fluorescence efficiency (Pandey *et al.* 2021; Elkun *et al.* 2024; Venkatesh *et al.* 2025). Microwave-assisted processing has attracted increasing interest due to its ability to deliver rapid, volumetric heating that accelerates carbonization while minimizing energy consumption and reaction time (Qu *et al.* 2012; Choi *et al.* 2017; Kumar *et al.* 2020). However, the optical performance of microwave-derived CQDs strongly depends on the rational selection of carbon precursors, dopant sources, and passivating agents, which collectively govern defect density and surface-state distribution.

To place these structure–property considerations into context, several studies have systematically examined how different synthetic strategies and precursor combinations influence the fluorescence quantum yield of CQDs. A growing body of literature demonstrates that fluorescence quantum yield in CQDs is highly sensitive to the combined effects of precursor molecular structure, dopant chemistry, and surface passivation strategy. Amphiphilic CQDs have been reported to show fluorescence quantum yields of ≤20% (Tan *et al.* 2016; Bhamore *et al.* 2018), which significantly constrains their practical utilization. This relatively low efficiency underscores that simple surface amphiphilicity alone is insufficient to suppress non-radiative recombination pathways, necessitating more deliberate control over dopant chemistry and surface states. Previous studies have reported the fabrication of CQDs via single-step microwave approaches using citric acid and thiourea in formamide, achieving moderate quantum yields (Venkatesh *et al.* 2025). In related work, highly luminescent S, N-co-doped carbon quantum dots synthesized from o-phenylenediamine and DL-DOPA achieved a quantum yield of approximately 17% under short microwave irradiation times (Venkatesh *et al.* 2025 a, b). It has also been shown that precursor composition and solvent environment critically influence emission behaviour, enabling the formation of blue- or green-emissive CQDs with quantum yields reaching up to ~42% (Qiao *et al.* 2020). Together, these reports reveal that enhanced quantum yield is not governed by a single parameter but arises from the coupled effects of dopant type, molecular precursor structure, reaction medium, and surface passivation strategy (Choi *et al.* 2017; Cui *et al.* 2021; Li *et al.* 2022; Barman *et al.* 2014). These studies collectively indicate that while nitrogen doping plays a central role in improving luminescence, its effectiveness is closely linked to precursor chemistry, reaction medium, and surface passivation rather than dopant incorporation alone (Lin *et al.* 2016; Tadesse *et al.* 2020; Liu *et al.* 2018; Ding *et al.* 2014)

Recent efforts have therefore shifted toward integrating heteroatom doping with intrinsic surface functionalization using small organic molecules or polymeric stabilizers (Choi *et al.* 2017; Tan *et al.* 2016; Ding *et al.* 2014; Kolanowska *et al.* 2022). Within this context, the choice of carbon precursor becomes critical, as precursor molecular structure directly governs dehydration pathways, nucleation behaviour, and the nature of surface functional groups formed during carbonization (Qiao *et al.* 2020; Stefanakis *et al.* 2014; Zhang *et al.* 2016; Zhu *et al.* 2009). Such systems facilitate controlled carbonization, suppress non-radiative defects, and generate diverse emissive surface states without requiring post-synthetic modification (Kumar *et al.* 2020; Li *et al.* 2022; Barman *et al.* 2014). Malic acid represents a strategically advantageous carbon precursor owing to its low molecular weight, biocompatibility, and the presence of multiple carboxyl and hydroxyl functionalities, which facilitate controlled dehydration, homogeneous nucleation, and the generation of oxygen-rich surface states during CQD formation (Xu *et al.* 2014; Mujahid, 2024; Cui *et al.* 2021). Ethanolamine serves as an efficient nitrogen source while simultaneously introducing amine-based surface states, whereas polyvinylpyrrolidone (PVP) acts

as a stabilizing and passivating polymer that enhances colloidal stability and emission efficiency (Ding *et al.* 2014; Choi *et al.* 2017; Kolanowska *et al.* 2022). The combined use of these components enables simultaneous control over composition, surface chemistry, and photophysical response, offering a platform to systematically establish structure–property relationships in nitrogen-doped CQDs (Barman *et al.* 2014; Cui *et al.* 2021).

Despite these advances, existing studies often address individual aspects such as quantum yield enhancement, green synthesis, or microwave processing in isolation, without fully developing an integrated structure–property framework that links sustainable precursor design, heteroatom incorporation, and photophysical performance (Qiao *et al.* 2020; Kumar *et al.* 2020; Mujahid, 2024). In this study, we employ malic acid, PVP, and ethanolamine to synthesize nitrogen-doped CQDs (denoted MPE-NCQDs) via a one-step microwave-assisted strategy. The approach enables rapid carbonization and surface modification while avoiding prolonged thermal treatments (Stefanakis *et al.* 2014; Zhang *et al.* 2016; Zhu *et al.* 2009). We systematically investigate the morphology, composition, surface chemistry, and photophysical behaviour of the resulting MPE-NCQDs using complementary analytical approaches. By correlating precursor chemistry, nanoscale structure, heteroatom incorporation, and photophysical response, this work is designed to address the combined gap of limited structure–property correlation in sustainable, microwave-assisted CQD systems, rather than focusing on quantum yield improvement alone.

2. EXPERIMENTAL PROCEDURE

2.1 Materials

Malic acid (MA, ≥99%), polyvinylpyrrolidone (PVP, MW ≈ 40,000), and ethanolamine (EA, ≥99%) were obtained from Sigma-Aldrich chemicals. Each reagent was utilised without subsequent purification, and DI water was employed in every stage of the experiments.

2.2 Characterization

Optical characterization of the MPE-NCQDs was performed using UV–visible absorption spectroscopy (Shimadzu UV-2450 PC) recorded over the 200–800 nm range, and steady-state photoluminescence spectroscopy (Horiba Jobin Yvon, Fluorolog-3) at ambient temperature. Time-resolved photophysical properties were examined by time-correlated single-photon counting (TCSPC) using pulsed excitation at 360 nm on a Horiba Fluoromax Plus system. Surface functional groups and chemical bonding environments were analysed by Fourier-transform infrared (FTIR) spectroscopy (BRUKER system) in the mid-infrared region. Morphological characterization was carried out using transmission electron microscopy (JEOL JEM-2100 PLUS, 200 kV) to determine particle shape, size distribution, and dispersion, while atomic force microscopy (NTEGRA Prima AFM, NT-MDT Technology), operated in semi-contact mode, was employed to probe surface topology and height profiles, with image analysis performed using Gwyddion software. Elemental composition and spatial distribution were examined by field-emission scanning electron microscopy (FE-SEM, SIGMA 300 GEMINI) equipped with an energy-dispersive X-ray (EDX) detector, providing complementary compositional information rather than morphological detail. Crystallographic characteristics were analysed using X-ray diffraction (Bruker D8 Advance) with Cu Kα radiation (λ = 1.5418 Å) at a step size of 0.02° under 2θ scanning mode.

2.3 Synthesis of MPE-NCQDs

Aqueous solutions of MA (3 g) and PVP (1 g) were prepared and combined with ethanolamine (5 mL) under continuous mixing to form a uniform precursor. The precursor solution was subjected to microwave irradiation (900 W) for 2.2 min, during which a dark brown coloration developed, indicating carbon dot formation (Zhu *et al.* 2009; Stefanakis *et al.* 2014; Zhang *et al.* 2016). After natural cooling, the reaction mixture was diluted with deionized water and centrifuged at 3500 rpm (corresponding to approximately 1500 × g) for 30 min. The supernatant was purified by dialysis using a 1000 Da cutoff membrane for 24 h, filtered through a 0.22 μm membrane, and dried at 60 °C to obtain the final MPE-NCQD powder.

2.4 Quantum Yield Determination

The fluorescence quantum yield (Φ) of the MPE-NCQDs was determined at an excitation wavelength of 360 nm by a relative method using quinine sulphate in 0.1 M H_2SO_4 as the reference fluorophore (Li *et al.* 2010; Esfandiari *et al.* 2019). The aqueous dispersion of MPE-NCQDs and the reference solution were diluted to maintain a low absorbance (A < 0.1) at the excitation wavelength to minimize inner-filter effects. Fluorescence spectra were recorded under identical instrumental conditions, with all measurements performed in triplicate, and the integrated emission intensity was plotted as a function of absorbance. The quantum yield was calculated using the following equation, and the reported values represent the mean ± standard deviation obtained from three independent measurements:

$$\Phi_s = \Phi_r \left(\frac{I_s}{I_r}\right)\left(\frac{A_r}{A_s}\right)\left(\frac{n_s}{n_r}\right)^2 \quad \ldots (1)$$

where Φ_r and Φ_s denote the quantum yields of the reference and sample, respectively; I_r and I_s

correspond to the integrated fluorescence intensities; A_r and A_s represent the absorbance at the excitation wavelength; and n_r and n_s denote the refractive indices of the respective solvents.

3. RESULTS AND DISCUSSION

3.1 Fabrication and Structural Elucidation of MPE-NCQDs

The MPE-NCQDs were successfully developed via the single-step microwave-assisted approach utilising MA, PVP, and EA as carbon as well as nitrogen sources, as depicted in Scheme 1. The schematic illustrates the sequential processes of precursor dehydration, polymer-assisted carbonization, and simultaneous nitrogen incorporation under microwave irradiation, highlighting the role of PVP and ethanolamine in surface passivation and defect-state formation (Zhu *et al.* 2009; Stefanakis *et al.* 2014; Zhang *et al.* 2016).



Scheme 1: Illustrative schematic for MPE-NCQD formation via a one-pot microwave-driven route

The microwave-assisted route enables rapid carbonization and passivation within minutes, providing a uniform and efficient synthesis pathway for highly fluorescent carbon dots. This rapid, volumetric heating is particularly effective in promoting simultaneous carbonization and surface passivation, which helps suppress non-radiative defect formation at early stages of nucleation (Kumar *et al.* 2020; Cui *et al.* 2021). The morphological characteristics of MPE-NCQDs were examined utilising TEM. As represented in Figure 1(a–b), the obtained nanoparticles were approximately spherical, monodispersed, and well separated, indicating effective surface passivation by PVP- and ethanolamine-derived functional groups (Ding *et al.* 2014; Choi *et al.* 2017). The lack of clearly resolved lattice fringes in the high-resolution TEM micrograph points to a non-crystalline carbon structure, a characteristic feature frequently associated with doped CQDs. This observation reflects short-range ordering at the nanoscale rather than long-range crystallinity (Zhai *et al.* 2012; Cui *et al.* 2021). The size distribution histogram of the nanoparticles (Figure 1(d)) revealed an average particle diameter of nearly 3.6 nm, indicating the nanoscale nature of the MPE-NCQDs (Venkatesh *et al.* 2025). Such small dimensions favour quantum confinement effects, which are known to contribute to size-dependent optical transitions in carbon-based quantum dots (Li *et al.* 2010; Barman *et al.* 2014).

The thickness of MPE-NCQDs was further evaluated by AFM, and the height profile demonstrated that the average thickness of the particles was around 6.6 nm (Figure 1(c) and 1(f)), suggestive of stacked or multilayer-like carbon domains formed during microwave carbonization, rather than definitive multilayered graphene-like structures (Stefanakis *et al.* 2014; Cui *et al.* 2021). The elemental constituents of the MPE-NCQDs were examined by EDX spectroscopy, as represented in Figure 1(e). The EDX analysis revealed carbon (73.97 wt.%, 75.23 atomic %), nitrogen (11.26 wt.%, 10.55 atomic %), and oxygen (14.77 wt.%, 14.22 atomic %) as the dominant elements, confirming effective nitrogen doping within the carbon matrix along with the presence of oxygen-based surface moieties (Lin *et al.* 2016; Tadesse *et al.* 2020). The coexistence of O, C, and N elements indicates that the MPE-NCQDs are rich in hydrophilic surface groups, contributing to their excellent aqueous dispersibility and optical behaviour. These surface functionalities also act as emissive or passivating sites, linking the observed composition directly to the photoluminescence behaviour discussed in the subsequent section (Barman *et al.* 2014; Li *et al.* 2022). Minor variations between the elemental compositions obtained from EDX and XPS analyses can be attributed to their fundamentally different probing depths, with EDX providing bulk-sensitive information while XPS selectively reflects surface-enriched heteroatom distributions (Esfandiari *et al.* 2019; Cui *et al.* 2021).

Moreover, the crystallographic nature of the MPE-NCQDs was examined by XRD analysis. As represented in Figure 2(a), a broad diffraction feature appearing around $2\theta \approx 26.7°$ was detected and assigned to the (002) reflection of graphitic carbon. The corresponding broad peak signifies the presence of amorphous or turbostratic carbon, providing complementary evidence of limited long-range order in the carbon framework, which is consistent with the TEM findings and previous literature reports (Li *et al.* 2020, Zhou *et al.* 2022). The observed pattern confirms partial

graphitic ordering within an amorphous matrix, typical of heteroatom-doped CQDs. This interpretation is further supported by the SAED pattern (Figure 2(c)), which displays diffuse concentric rings rather than sharp diffraction spots, indicating the absence of long-range crystallinity and reinforcing the amorphous or turbostratic nature of the MPE-NCQDs (Stefanakis *et al.* 2014; Cui *et al.* 2021).

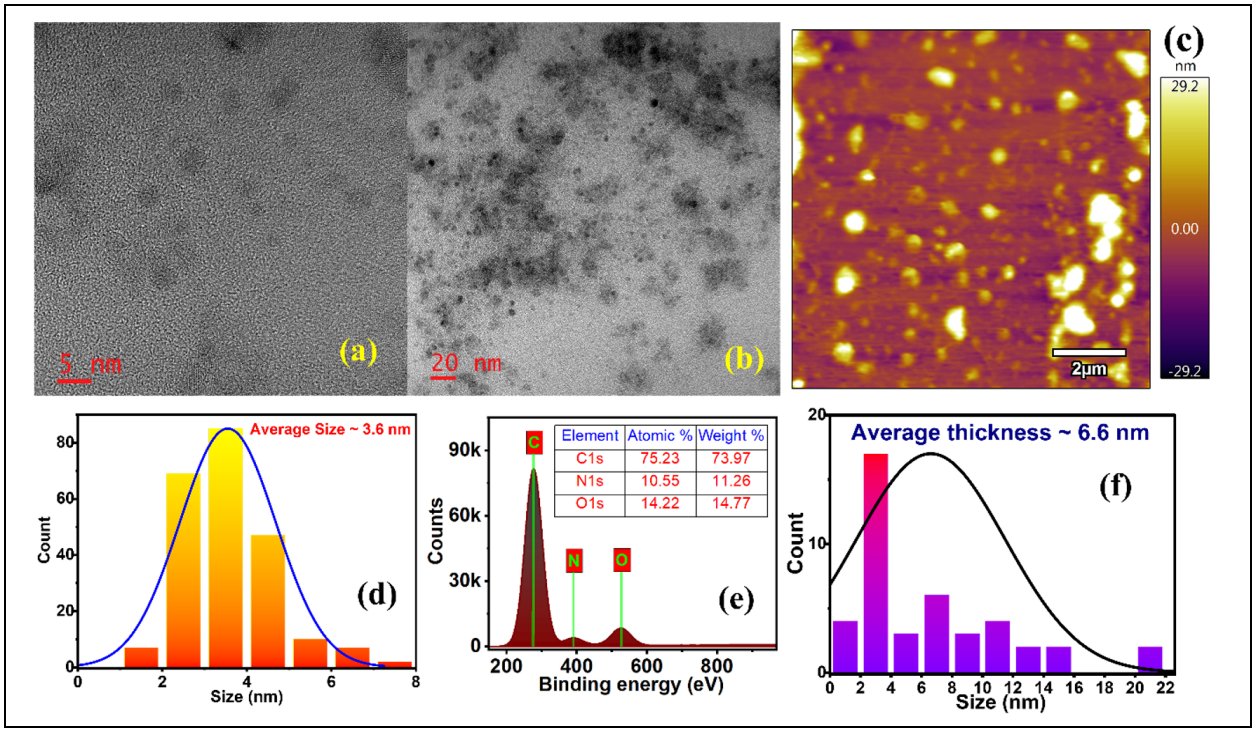


Fig. 1: (a, b) TEM images represented the morphology of MPE-NCQDs, (c) AFM image depicted the surface topology, (d) histogram obtained from TEM images showed particle size distribution, (e) EDX spectrum represented elemental composition and (f) histogram of height profile showed the thickness of MPE-NCQDs

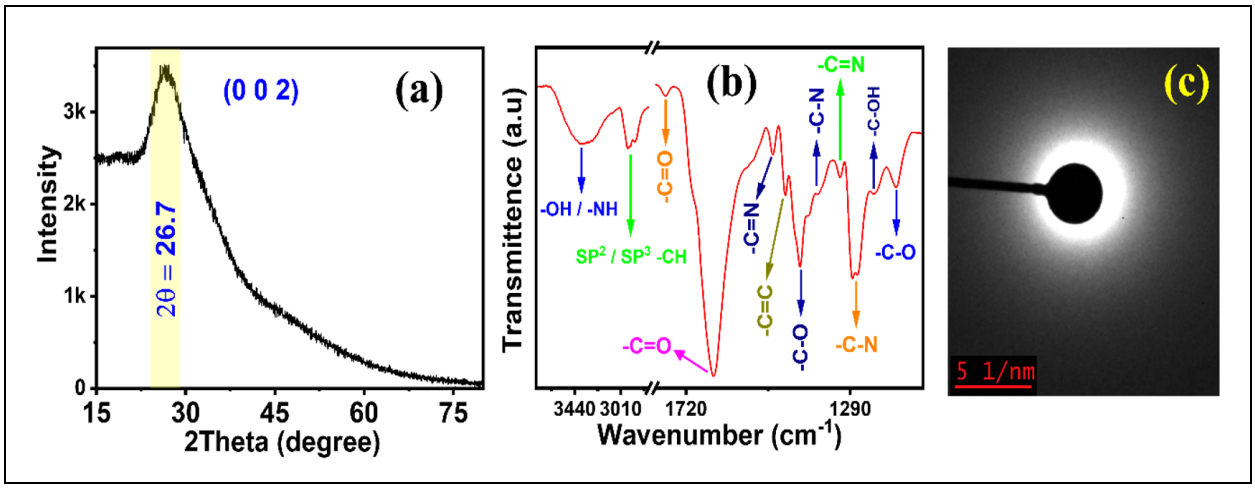


Fig. 2: (a) XRD pattern represented the amorphous nature of MPE-NCQDs, (b) FTIR spectrum depicted the various surface functional groups and (c) SAED pattern showed the diffraction features of the synthesized MPE-NCQDs

The surface functional moieties of the MPE-NCQDs were examined using FTIR spectroscopy (Figure 2(b)). The FTIR spectrum exhibited a broad absorption band around 3393 cm^{-1}, indicating N–H or O–H stretching vibrations, confirming the existence of amine or hydroxyl moieties (Kim *et al.* 2017; Bera *et al.* 2018; Li *et al.* 2022, Huang *et al.* 2024). The prominent vibrational bands at 2945, 2919, and 2874 cm^{-1} are assigned to sp^2/sp^3 C–H stretching vibrations. A weak peak at 1774 cm^{-1} represents the carbonyl stretching of O–C=O groups, while a prominent band at 1648 cm^{-1} indicates C=O stretching of amide (CONH) groups.

Additional peaks observed at 1492 cm^{-1} indicate C=N stretching, while the band near 1460 cm^{-1} arises from C=C skeletal vibrations.

For a comprehensive assessment of surface elemental composition, valence states, and chemical bonding environments, X-ray photoelectron spectroscopy (XPS) analysis was performed, as shown in Figure 3. The survey XPS spectrum (Figure 3a) reveals three dominant signals corresponding to carbon, nitrogen, and oxygen, confirming the successful incorporation of heteroatoms within the carbon framework (Zhai *et al.* 2012; Cui *et al.* 2021). The characteristic core-level peaks located at binding energies of approximately 285 eV, 399 eV, and 531 eV are assigned to C 1s, N 1s, and O 1s, respectively. Quantitative analysis of the survey spectrum indicates that the MPE-NCQDs consist of approximately 73.61 atomic % carbon (71.15 wt.%), 11.18 atomic % nitrogen (12.77 wt.%), and 15.21 atomic % oxygen (16.09 wt.%), suggesting effective nitrogen doping together with oxygen-rich surface functionalization, rather than bulk compositional dominance.

The high-resolution C 1s spectrum (Figure 3b) can be deconvoluted into four distinct components centred at ~284.9, 285.9, 287.7, and 289.2 eV, corresponding to sp^2-hybridized graphitic carbon (C=C/C–C), sp^3 carbon bonded to heteroatoms (C–N/C–O), carbonyl or imine groups (C=O/C=N), and carboxyl or ester functionalities (O=C–O), respectively (Barman *et al.* 2014; Kolanowska *et al.* 2022). These features indicate the coexistence of conjugated carbon domains and heteroatom-derived surface functionalities, which are known to play a critical role in governing emissive behaviour in carbon-based quantum dots.

The N 1s core-level spectrum (Figure 3c) exhibits two primary components located at approximately 399.8 and 401.0 eV, which are attributed to pyrrolic nitrogen (C_2–N–H) and graphitic nitrogen (N–C_3), respectively (Lin *et al.* 2016; Shan *et al.* 2021). Pyrrolic nitrogen is generally associated with defect-related emissive sites, whereas graphitic nitrogen contributes to modulation of the electronic structure of the carbon core, together influencing the observed photoluminescence behaviour.

The O 1s spectrum (Figure 3d) displays two major peaks at ~531.5 and 532.8 eV, assigned to carbonyl (C=O) and hydroxyl/ether (C–OH/C–O–C) functionalities, respectively (Saljoughi *et al.* 2020; Huang *et al.* 2024). The presence of these oxygen-containing groups supports the FTIR results and indicates a hydrophilic, passivated surface chemistry consistent with the observed aqueous dispersibility of the MPE-NCQDs.

In combination with the EDX analysis, these findings highlight the distinction between bulk-sensitive (EDX) and surface-sensitive (XPS) compositional information, explaining minor discrepancies between the two techniques. Overall, the revised XPS analysis shifts the discussion from a purely descriptive listing of spectral features to an interpretative framework, emphasizing the role of surface chemistry and heteroatom configuration in regulating the photophysical properties of the MPE-NCQDs.

3.2 Photophysical Investigation

To examine the photophysical characteristics of the MPE-NCQDs, steady-state and time-resolved spectroscopic analyses were performed. The absorption and emission spectra of the MPE-NCQDs dispersed in water are shown in Figure 4(a). The absorption profile displays two distinct bands centred at approximately 228 and 360 nm. The sharp peak at 228 nm is attributed to the $\pi \rightarrow \pi^*$ transition of aromatic sp^2 carbon domains (C=C), while the broader band around 360 nm originates from the $n \rightarrow \pi^*$ transition associated with surface carbonyl (C=O) or imine (C=N) functional groups (Bera *et al.* 2018). Similar absorption features have been widely reported for heteroatom-doped carbon quantum dots synthesized via microwave and hydrothermal routes, where π–π^* transitions arise from graphitic sp^2 cores and n–π transitions are associated with surface defect or heteroatom-containing functional states, thereby supporting the assignments made here (Li *et al.* 2010; Zhai *et al.* 2012; Cui *et al.* 2021).

The corresponding excitation and emission spectra reveal a strong emission centred at ~460 nm upon excitation at 360 nm, with a photoluminescence quantum yield of approximately 42% (Figure 4(a), Table 1). These optical features suggest the coexistence of graphitic cores and surface defect states that are likely to contribute to radiative recombination in the MPE-NCQDs (Barman *et al.* 2014; Liu *et al.* 2018). Under UV illumination, the aqueous dispersion of MPE-NCQDs exhibits bright photoluminescence, whereas under ambient light it appears orange-to-red, demonstrating strong emissive behaviour (Scheme 1).

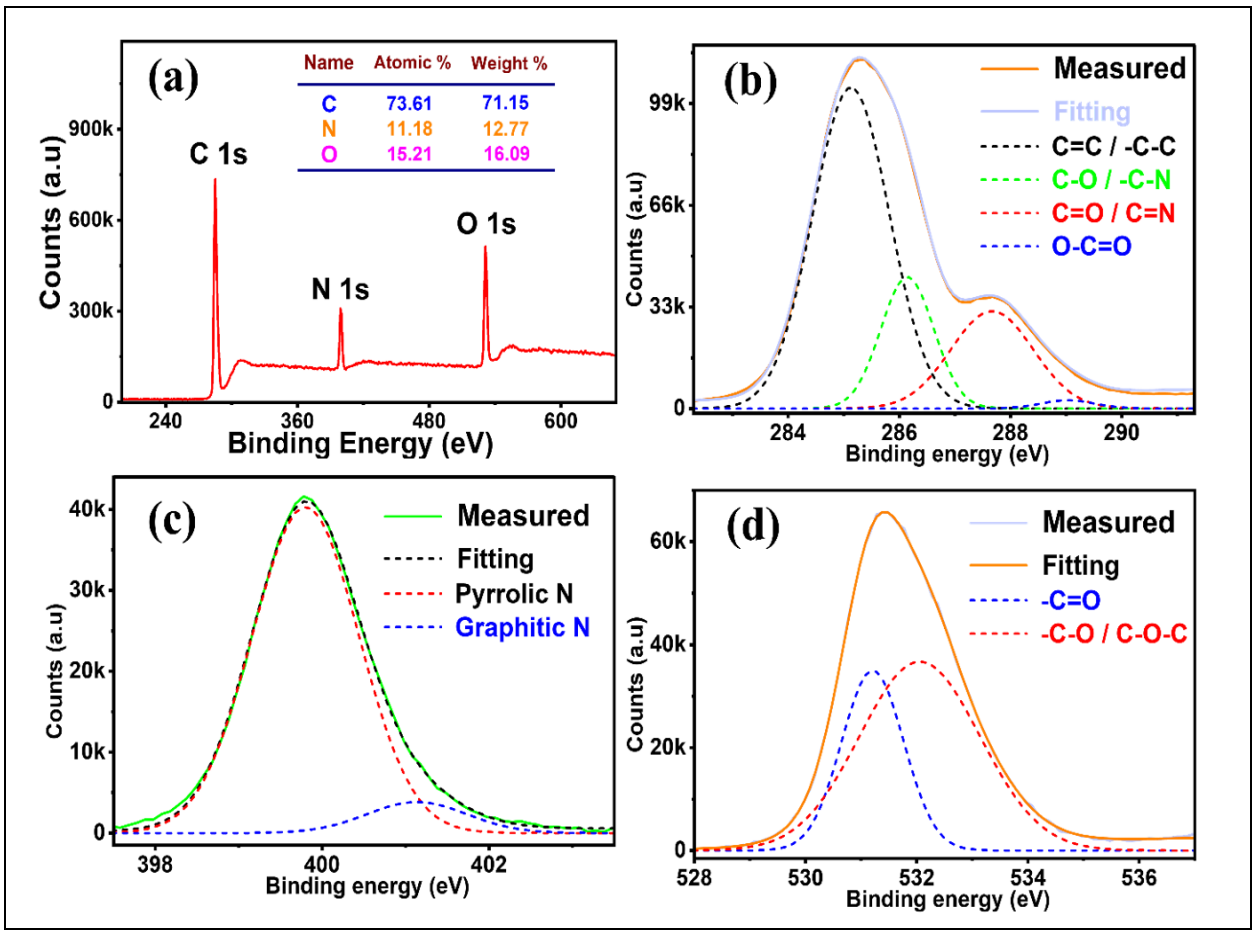


Fig. 3: (a) XPS survey spectrum illustrated the elemental composition of MPE-NCQDs, while deconvoluted high-resolution spectra of (b) C1s, (c) N1s and (d) O1s represented the detailed chemical bonding states

The PL spectra recorded at various excitation wavelengths (Figure 4(b)) exhibit clear excitation-dependent emission behaviour. As the excitation wavelength is increased from 260 to 550 nm, the emission maxima gradually red-shift with a concomitant decrease in intensity. This behaviour is further supported by the normalized PL spectra shown in Figure 4(c), confirming the wavelength-dependent shift. Such excitation-dependent photoluminescence is a characteristic feature of carbon quantum dots and is generally attributed to the presence of multiple emissive centers associated with surface states and defect sites (Puvvada *et al.* 2012; Wang *et al.* 2020). The observed PL behaviour can be rationalized by the synergistic contribution of quantum confinement effects within the sp^2 carbon domains and surface-state-mediated electronic transitions. The presence of nitrogen- and oxygen-containing functional groups introduces localized energy levels within the bandgap, resulting in excitation-dependent emission characteristics (Zhu *et al.* 2009; Chandra *et al.* 2011; Puvvada *et al.* 2012; Zhai *et al.* 2012; Ma *et al.* 2012). Additional effects such as interlayer charge transfer, excitonic coupling, and solvent–surface interactions may further modulate the optical response (Li *et al.* 2022; Barman *et al.* 2014).

Table 1. Determined quantum yield (QY) of the as-prepared MPE-NCQDs

Sample	Integrated PL Intensity (I)	Abs. at 360 nm (A)	Refractive Index of Solvent (n)	Quantum Yield at 360 nm
Quinine Sulphate	65742.33	0.079	1.33	54%
MPE-NCQDs	50658.74	0.078	1.33	42%

Fluorescence decay dynamics were further investigated by TCSPC using 360 nm excitation, as depicted in Figure 4(d). The decay profile follows a biexponential model comprising a fast decay component (τ_1 = 3.06 ns, 35%) and a slower decay component (τ_2 = 9.48 ns, 65%). The shorter lifetime component is attributed to recombination within the graphitic core, whereas the longer component is associated with surface defect or trap-state relaxation processes (Bel *et al.* 2014; Flak *et al.* 2018; Shen *et al.* 2018; Rodrigues *et al.* 2021). Comparable biexponential lifetimes, typically ranging from a few nanoseconds to ~10 ns, have been widely reported for nitrogen-doped carbon quantum dots, where shorter lifetime components arise from core-state

recombination and longer components originate from surface- or defect-related states, indicating that the decay dynamics observed here are consistent with established N-CQD photophysical behaviour (Shen *et al.* 2018; Rodrigues *et al.* 2021). The quality of the biexponential fitting was confirmed by a reduced chi-square (χ^2) value of 0.9878, indicating excellent agreement between the experimental decay profile and the fitted model.

Collectively, the steady-state and time-resolved photophysical analyses indicate that the MPE-NCQDs possess multiple emissive centers, a relatively high photoluminescence quantum yield (~42%), and complex carrier relaxation dynamics, suggesting their potential suitability for optoelectronic and fluorescence-based sensing applications (Yuan *et al.* 2020; Wang *et al.* 2020).

The refractive index used for quantum yield calculations corresponds to that of the aqueous medium (n = 1.33), as all measurements were performed in water.

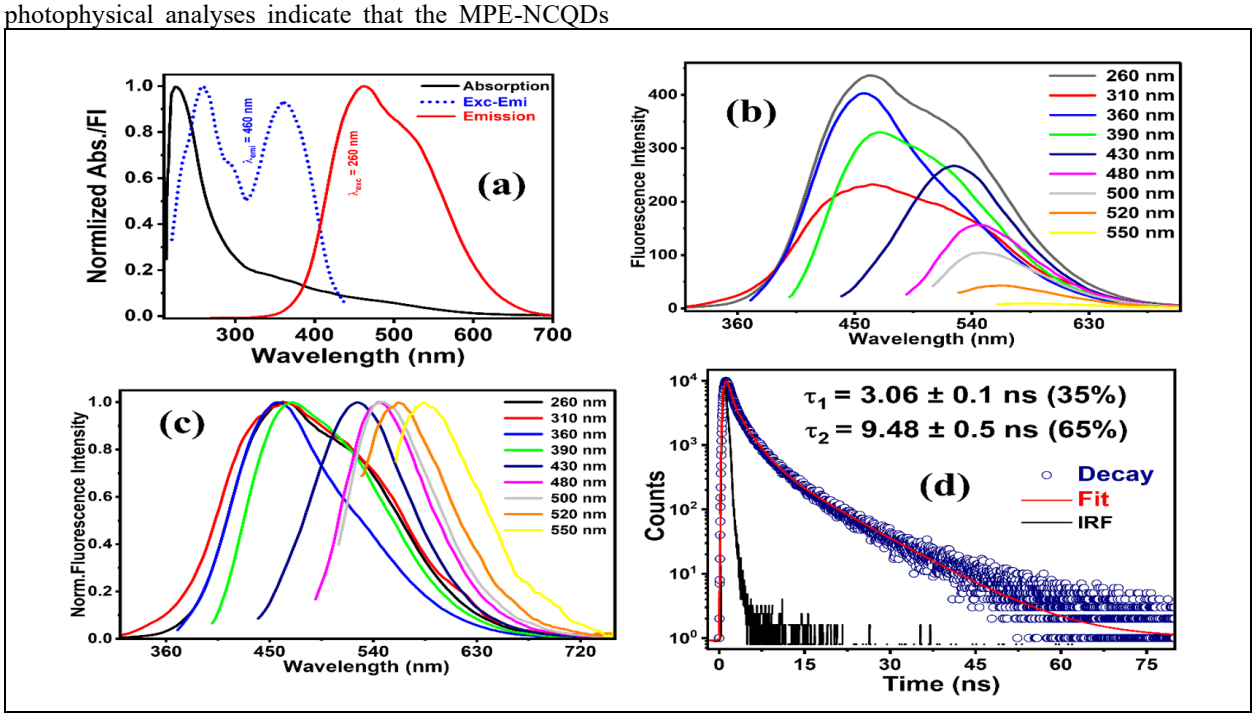


Fig. 4: Optical characterization of MPE-NCQDs in aqueous dispersion: (a) excitation, emission, and normalized absorption spectra; (b) emission spectra at multiple excitation wavelengths demonstrating excitation-dependent emission; (c) the normalized PL spectra; and (d) the lifetime decay profile of PL produced via TCSPC upon 360 nm excitation

4. SUMMARY

We have successfully fabricated a facile one-step microwave-assisted approach for synthesizing MPE-NCQDs using malic acid, PVP, and ethanolamine. The as-prepared nanoparticles exhibit uniform nanoscale dimensions with effective heteroatom incorporation and abundant surface functionalization, leading to stable and well-dispersed carbon quantum dots (Choi *et al.* 2017; Cui *et al.* 2021). Structural analyses confirm partially graphitic domains embedded within an amorphous carbon matrix enriched with surface functionalities, which are characteristic of heteroatom-doped CQDs (Zhai *et al.* 2012; Ding *et al.* 2014).

Optically, the MPE-NCQDs display efficient photoluminescence with a relatively high quantum yield and excitation-dependent emission behaviour, reflecting the interplay between nanoscale carbon domains and surface functionalization (Barman *et al.* 2014; Li *et al.* 2022). These features highlight the role of precursor chemistry, heteroatom doping, and surface passivation in regulating the emission behaviour of the MPE-NCQDs, rather than isolated structural parameters alone (Cui *et al.* 2021; Wang *et al.* 2020).

Overall, the results suggest that MPE-NCQDs are promising candidates for optoelectronic, sensing, and biocompatible fluorescence applications (Yuan *et al.* 2020; Liu *et al.* 2018), while future studies will focus on establishing structure–property correlations under device-relevant conditions, improving emission stability under continuous excitation, and evaluating sensing performance in complex aqueous environments.

ACKNOWLEDGMENTS

T.A.R., Y.V., A.V.R., and N.S.R. gratefully acknowledge the Principal, Dr. V. S. Krishna Government Degree College (Autonomous), Visakhapatnam, for providing the necessary research laboratory facilities

AUTHOR CONTRIBUTION

Thutipati Appa Rao: Conceptualization, methodology, Experimental work, data analysis, data acquisition, result interpretation, and manuscript writing;

Yeduru Venkatesh: Conceptualization, methodology, Experimental work, data analysis, data acquisition, result interpretation, and manuscript writing, Review and editing, supervision;

Bonige Kishore Babu: Review and editing, supervision;

Adari Venkata Ramesh: Data analysis, data acquisition, and result interpretation;

N. Sankara Rao: Data analysis, data acquisition, and result interpretation;

R. Ramesh Naidu: Data analysis, data acquisition, and result interpretation.

FUNDING

This research received no specific grant from any funding agency in the public, commercial, or not-for-profit sectors.

CONFLICTS OF INTEREST

The authors declare that there is no conflict of interest.

COPYRIGHT

This article is an open-access article distributed under the terms and conditions of the Creative Commons Attribution (CC BY) license (http://creativecommons.org/licenses/by/4.0/).

REFERENCES

Atchudan, R., Edison, T. N. J. I., Perumal, S., Muthuchamy, N. and Lee, Y. R., Hydrophilic nitrogen-doped carbon dots from biowaste using dwarf banana peel for environmental and biological applications, *Fuel*, 275, 117821 (2020). https://doi.org/10.1016/j.fuel.2020.117821

Barman, M. K., Jana, B., Bhattacharyya, S. and Patra, A., Photophysical properties of doped carbon dots (N, P and B) and their influence on electron/hole transfer in carbon dots–nickel (II) phthalocyanine conjugates, *J. Phys. Chem. C*, 118(34), 20034–20041 (2014). https://doi.org/10.1021/jp507080c

Bel, H. M. N., Haouari, M., Zaaboub, Z., Nafoutti, M., Hassen, F. and Maaref, H., Time resolved and temperature dependence of the radiative properties of thiol-capped CdS nanoparticles films, *J. Nanopart. Res.*, 16(3), 2242 (2014). https://doi.org/10.1007/s11051-013-2242-9

Bera, M., Chandravati, N., Gupta, P. and Maji, P. K., Facile one-pot synthesis of graphene oxide by sonication assisted mechanochemical approach and its surface chemistry, *J. Nanosci. Nanotechnol.*, 18(2), 902–912 (2018). https://doi.org/10.1166/jnn.2018.14306

Bhamore, J. R., Jha, S., Park, T. J. and Kailasa, S. K., Fluorescence sensing of Cu^{2+} ion and imaging of fungal cell by ultra-small fluorescent carbon dots derived from Acacia concinna seeds, *Sens. Actuators B Chem.*, 277, 47–54 (2018). https://doi.org/10.1016/j.snb.2018.08.149

Chandra, S., Das, P., Bag, S., Laha, D. and Pramanik, P., Synthesis, functionalization and bioimaging applications of highly fluorescent carbon nanoparticles, *Nanoscale*, 3(4), 1533–1540 (2011). https://doi.org/10.1039/c0nr00735h

Choi, Y., Jo, S., Chae, A., Kim, Y. K., Park, J. E., Lim, D., Park, S. Y. and In, I., Simple microwave-assisted synthesis of amphiphilic carbon quantum dots from A_3/B_2 polyamidation monomer set, *ACS Appl. Mater. Interf.*, 9(33), 27883–27893 (2017). https://doi.org/10.1021/acsami.7b06066

Cui, L., Ren, X., Sun, M., Liu, H. and Xia, L., Carbon dots: synthesis, properties and applications, *Nanomater.*, 11(12), 3419 (2021). https://doi.org/10.3390/nano11123419

Derfus, A. M., Chan, W. C. W. and Bhatia, S. N., Probing the cytotoxicity of semiconductor quantum dots, *Nano Lett.*, 4(1), 11–18 (2004). https://doi.org/10.1021/nl0347334

Ding, H., Zhang, P., Wang, T. Y., Kong, J. L. and Xiong, H. M., Nitrogen-doped carbon dots derived from polyvinyl pyrrolidone and their multicolor cell imaging, *Nanotechnol.*, 25(20), 205604 (2014). https://doi.org/10.1088/0957-4484/25/20/205604

Ding, H., Zhou, X., Qin, B., Zhou, Z. and Zhao, Y., Highly fluorescent near-infrared emitting carbon dots derived from lemon juice and its bioimaging application, *J. Lumin.*, 211, 298–304 (2019). https://doi.org/10.1016/j.jlumin.2019.03.064

Elkun, S., Ghali, M., Sharshar, T. and Mosaad, M. M., Green synthesis of fluorescent N-doped carbon quantum dots from castor seeds and their applications in cell imaging and pH sensing, *Sci. Rep.*, 14(1), 27927 (2024). https://doi.org/10.1038/s41598-024-78745-0

Esfandiari, N., Bagheri, Z., Ehtesabi, H., Fatahi, Z., Tavana, H. and Latifi, H., Effect of carbonization degree of carbon dots on cytotoxicity and photo-induced toxicity to cells, *Heliyon*, 5(11), e02940 (2019). https://doi.org/10.1016/j.heliyon.2019.e02940

Flak, D., Przysiecka, Ł., Nowaczyk, G., Scheibe, B., Kościński, M. and Jesionowski, T., GQDs-MSNs nanocomposite nanoparticles for simultaneous intracellular drug delivery and fluorescent imaging, *J. Nanopart. Res.*, 20(11), 306 (2018). https://doi.org/10.1007/s11051-018-4416-y

Huang, J., Klahn, M., Tian, X., Dai, X., Rabeah, J., Corzilius, B., Stephan, B., Lund, H., Norbert, S., Tim, P., Andrew, L. J., Jiao, H. and Strunk, J. and Aladin, V., Exfoliated polymeric carbon nitride nanosheets for photocatalytic applications, *ACS Appl. Nano Mater.*, 7(7), 7442–7452 (2024). https://doi.org/10.1021/acsanm.4c00133

Kim, J., Kim, S. W., Yun, H. and Kim, B. J., Impact of size control of graphene oxide nanosheets for enhancing electrical and mechanical properties of carbon nanotube–polymer composites, *RSC Adv.*, 7(48), 30221–30228 (2017). https://doi.org/10.1039/C7RA04015F

Kolanowska, A., Dzido, G., Krzywiecki, M., Tomczyk, M. M., Łukowiec, D. and Ruczka, S., Carbon quantum dots from amino acids revisited: survey of renewable precursors toward high quantum-yield blue and green fluorescence, *ACS Omega*, 7(45), 41165–41176 (2022). https://doi.org/10.1021/acsomega.2c04751

Kumar, P., Bhatt, G., Kaur, R., Dua, S. and Kapoor, A., Synthesis and modulation of the optical properties of carbon quantum dots using microwave radiation, *Fuller. Nanotub. Carbon Nanostruct.*, 28(9), 724–731 (2020). https://doi.org/10.1080/1536383X.2020.1752679

Li, H., He, X., Kang, Z., Huang, H., Liu, Y. and Liu, J., Water-soluble fluorescent carbon quantum dots and photocatalyst design, *Angew. Chem. Int. Ed.*, 49(26), 4430–4434 (2010). https://doi.org/10.1002/anie.200906154

Li, H., Su, D., Gao, H., Yan, X., Kong, D., Liu, X., Wang, C., Lu, G. and Jin, R., Design of red emissive carbon dots: robust performance for analytical applications in pesticide monitoring, *Anal. Chem.*, 92(4), 3198–3205 (2020). https://doi.org/10.1021/acs.analchem.9b04917

Li, P., Xue, S., Sun, L., Zong, X., An, L., Wang, X., Sun, Z. and Qu, D., Formation and fluorescent mechanism of red emissive carbon dots from o-phenylenediamine and catechol system, *Light Sci. Appl.*, 11(1), 298 (2022). https://doi.org/10.1038/s41377-022-00984-5

Lin, Y., Yao, B., Huang, T., Zhang, S., Cao, X. and Weng, W., Selective determination of free dissolved chlorine using nitrogen-doped carbon dots as a fluorescent probe, *Microchim. Acta*, 183(7), 2221–2227 (2016). https://doi.org/10.1007/s00604-016-1855-y

Liu, H., Li, Z., Sun, Y., Geng, X., Hu, Y., Meng, H., Ge, J., Qu, L. and Meng, H., Synthesis of luminescent carbon dots with ultrahigh quantum yield and inherent folate receptor-positive cancer cell targetability, *Sci. Rep.*, 8(1), 1086 (2018). https://doi.org/10.1038/s41598-018-19373-3

Lu, J., Yeo, P. S. E., Gan, C. K., Wu, P. and Loh, K. P., Transforming C60 molecules into graphene quantum dots, *Nat. Nanotechnol.*, 6(4), 247–252 (2011). https://doi.org/10.1038/nnano.2011.30

Ma, Z., Ming, H., Huang, H., Liu, Y. and Kang, Z., One-step ultrasonic synthesis of fluorescent N-doped carbon dots from glucose and their visible-light sensitive photocatalytic ability, *New J. Chem.*, 36(4), 861–864 (2012). https://doi.org/10.1039/C2NJ20942J

Mujahid, M., A simple green synthesis of carbon quantum dots from Prunus armeniaca and their application as fluorescent probes for the selective and sensitive detection of Cd^{2+} metal ion, *Mater. Res. Express*, 11(9), 095007 (2024). https://doi.org/10.1088/2053-1591/ad7921

Pandey, A., Devkota, A., Sigdel, A., Yadegari, Z., Dumenyo, K. and Taheri, A., Citric acid/β-alanine carbon dots as a novel tool for delivery of plasmid DNA into E. coli cells, *Sci. Rep.*, 11(1), 23964 (2021). https://doi.org/10.1038/s41598-021-03437-y

Puvvada, N., Kumar, B. N. P., Konar, S., Kalita, H., Mandal, M. and Pathak, A., Synthesis of biocompatible multicolor luminescent carbon dots for bioimaging applications, *Sci. Technol. Adv. Mater.*, 13(4), 045008 (2012). https://doi.org/10.1088/1468-6996/13/4/045008

Qi, H., Qiu, L., Zhang, X., Yi, T., Jing, J., Sitah, A. F., Zahrah, A., Aljabri, M. D., Rahman, M. M. and Sami, R., Novel N-doped carbon dots derived from citric acid and urea: fluorescent sensing for determination of metronidazole and cytotoxicity studies, *RSC Adv.*, 13(5), 2663–2671 (2023). https://doi.org/10.1039/D2RA07150A

Qiao, G., Chen, G., Wen, Q., Liu, W., Gao, J., Wang, Q. and Yu, Z., Rapid conversion from common precursors to carbon dots in large scale: spectral controls, optical sensing, cellular imaging and LEDs application, *J. Colloid Interf. Sci.*, 580, 88–98 (2020). https://doi.org/10.1016/j.jcis.2020.07.034

Qu, S., Wang, X., Lu, Q., Liu, X. and Wang, L., A biocompatible fluorescent ink based on water-soluble luminescent carbon nanodots, *Angew. Chem. Int. Ed.*, 51(49), 12215–12218 (2012). https://doi.org/10.1002/anie.201206791

Rodrigues, L. S., Sonsin, A. F., Barbosa, C. D. A. S., Oliveira, D. M. F., Fonseca, E. J. S., Santos, A. R., Costa, L. M. M. and Dornelas, C. B., An eco-friendly green and facile synthesis of carbon dots from red propolis wax with photoluminescence dependent of reaction time and thermal treatment in solid state, *J. Nanopart. Res.*, 23(11), 262 (2021). https://doi.org/10.1007/s11051-021-05362-7

Saljoughi, H., Khakbaz, F. and Mahani, M., Synthesis of folic acid conjugated photoluminescent carbon quantum dots with ultrahigh quantum yield for targeted cancer cell fluorescence imaging, *Photodiagn. Photodyn. Ther.*, 30, 101687 (2020). https://doi.org/10.1016/j.pdpdt.2020.101687

Sarkar, S., Gandla, D., Venkatesh, Y., Bangal, P. R., Ghosh, S., Misra, S. and Yang, Y., Graphene quantum dots from graphite by liquid exfoliation showing excitation-independent emission, fluorescence upconversion and delayed fluorescence, *Phys. Chem. Chem. Phys.*, 18(31), 21278–21287 (2016). https://doi.org/10.1039/C6CP01528J

Sasikumar, K., Rajamanikandan, R. and Ju, H., Inner filter effect-based highly sensitive quantification of 4-nitrophenol by strong fluorescent N, S co-doped carbon dots, *Carbon Lett.*, 34(3), 851–863 (2024). https://doi.org/10.1007/s42823-023-00666-1

Shan, F., Xia, H., Xie, X., Fu, L., Yang, H., Zhang, Y., Wang, Z., Yu, X. and Zhou, Q., Novel N-doped carbon dots prepared via citric acid and benzoylurea by green synthesis for high selectivity Fe(III) sensing and imaging in living cells, *Microchem. J.*, 167, 106273 (2021). https://doi.org/10.1016/j.microc.2021.106273

Shen, Y., Liang, Y., Wang, Y., Liu, C. and Ren, X., A comparative study on impact factors of emission: surface state, carbonaceous core and size based on series of exactly designed P, S co-doped carbon dots, *J. Nanopart. Res.*, 20(8), 229 (2018). https://doi.org/10.1007/s11051-018-4334-z

Stefanakis, D., Philippidis, A., Sygellou, L., Filippidis, G., Ghanotakis, D. and Anglos, D., Synthesis of fluorescent carbon dots by a microwave heating process: structural characterization and cell imaging applications, *J. Nanopart. Res.*, 16(9), 2646 (2014). https://doi.org/10.1007/s11051-014-2646-1

Tadesse, A., Hagos, M., RamaDevi, D., Basavaiah, K. and Belachew, N., Fluorescent nitrogen-doped carbon quantum dots derived from citrus lemon juice: green synthesis, mercury (II) ion sensing and live cell imaging, *ACS Omega*, 5(8), 3889–3898 (2020). https://doi.org/10.1021/acsomega.9b03175

Tan, J., Zhang, J., Li, W., Zhang, L. and Yue, D., Synthesis of amphiphilic carbon quantum dots with phosphorescence properties and their multifunctional applications, *J. Mater. Chem. C*, 4(42), 10146–10153 (2016). https://doi.org/10.1039/C6TC03027K

Venkatesh, Y., Naidu, P. V. S., Ramanjaneyulu, M., Rao, P. A. and Kundrapu, D. B., Synthesis of multifunctional sulfur-nitrogen co-doped carbon quantum dots via facile one-pot microwave-assisted synthesis: applications on antioxidant, antimicrobial activities and Fe^{3+} ion sensing, *J. Nanopart. Res.*, 27(2), 62 (2025). https://doi.org/10.1007/s11051-025-06260-y

Venkatesh, Y., Naidu, P. V. S., Rao, P. A. and Kundrapu, D. B., Green synthesis of multifunctional nitrogen-doped carbon quantum dots derived from citrus lemon juice: applications on antioxidant and antimicrobial activities and highly selective detection for Fe^{3+} ion sensing, *Res. Chem. Intermed.*, 51(5), 2621–2643 (2025). https://doi.org/10.1007/s11164-025-05567-8

Venkatesh, Y., Wadepalli, S., Bangal, P. R., Naidu, P. V. S. and Rao, P. A., Facile one-pot microwave-assisted synthesis and ultrafast spectroscopic characterization of nitrogen–sulfur co-doped carbon quantum dots, *Luminescence*, 40(2), e70108 (2025). https://doi.org/10.1002/bio.70108

Wang, L., Li, W., Yin, L., Liu, Y., Guo, H., Han, Y., Li, G., Li, M., Zhang, J., Vajtai, R., Ajayan, P. M., Wu, M. and Lai, J., Full-color fluorescent carbon quantum dots, *Sci. Adv.*, 6(41), eabb6772 (2020). https://doi.org/10.1126/sciadv.abb6772

Wu, H., Jiang, J., Gu, X. and Tong, C., Nitrogen and sulfur co-doped carbon quantum dots for highly selective and sensitive fluorescent detection of Fe (III) ions and L-cysteine, *Microchim. Acta*, 184(7), 2291–2298 (2017). https://doi.org/10.1007/s00604-017-2201-8

Xu, Y., Tang, C. J., Huang, H., Sun, C. Q., Zhang, Y. K., Wang, A. and Ye, Q. F., Green synthesis of fluorescent carbon quantum dots for detection of Hg^{2+}, *Chin. J. Anal. Chem.*, 42(9), 1252–1258 (2014). https://doi.org/10.1016/S1872-2040(14)60765-9

Yuan, F., Wang, Y. K., Sharma, G., Dong, Y., Zheng, X., Andrew, J., Golam, B., Fan, J. Z., Hao, K., Bin, C., Makhsud, A. I., Singh, K., Voznyy, O., Bakr, O. M., Lu, Z. H. and Sargent, E. H. and Li, P., Bright high-colour-purity deep-blue carbon dot light-emitting diodes via efficient edge amination, *Nat. Photonics*, 14(3), 171–176 (2020). https://doi.org/10.1038/s41566-019-0557-5

Zhai, X., Zhang, P., Liu, C., Bai, T., Li, W., Liu, W and Dai, L., Highly luminescent carbon nanodots by microwave-assisted pyrolysis, *Chem. Commun.*, 48(64), 7955–7957 (2012). https://doi.org/10.1039/C2CC33869F

Zhang, Y., Liu, X., Fan, Y., Guo, X., Zhou, L., Lin, J. and Lv, Y., One-step microwave synthesis of N-doped hydroxyl-functionalized carbon dots with ultra-high fluorescence quantum yields, *Nanoscale*, 8(29), 15281–15287 (2016). https://doi.org/10.1039/C6NR03125K

Zhou, H., Ren, Y., Li, Z., He, W. and Li, Z., Selective detection of Fe^{3+} by nitrogen–sulfur-doped carbon dots using thiourea and citric acid, *Coatings*, 12(8), 1042 (2022). https://doi.org/10.3390/coatings12081042

Zhu, H., Wang, X., Li, Y., Wang, Z., Yang, F. and Yang, X., Microwave synthesis of fluorescent carbon nanoparticles with electrochemiluminescence properties, *Chem. Commun.*, 45(34), 5118–5120 (2009). https://doi.org/10.1039/B907612C